Journal of Alloys and Compounds 507 (2010) 67–71

Contents lists available at ScienceDirect

Journal of Alloys and Compounds

journal homepage: www.elsevier.com/locate/jallcom

Peculiarity of component interaction in Er–Fe–Sn ternary system at 670 K and 770 K

L. Romaka*, V.V. Romaka, P. Demchenko, R. Serkiz

Ivan Franko L'viv National University, Kyryl & Mephodiy Str.6, 79005, L'viv, Ukraine

ARTICLE INFO

Article history:
Received 17 June 2010
Received in revised form 15 July 2010
Accepted 16 July 2010
Available online 14 August 2010

Keywords:
Intermetallics
Stannides
Phase diagrams
Crystal structure
X-ray diffraction

ABSTRACT

The isothermal sections of the phase diagram of Er–Fe–Sn ternary system were constructed at 770 and 670 K in the whole concentration range using X-ray and metallographic analyses. Component interaction in the Er–Fe–Sn system at 670 K results the existence of two ternary compounds, $ErFe_6Sn_6$ (YCo_6Ge_6-type) and $Er_5Fe_6Sn_{18}$ ($Tb_5Rh_6Sn_{18}$-type), while at 770 K only one intermediate $ErFe_6Sn_6$ phase was observed. The existence of the interstitial solid solution $ErFe_xSn_2$ (up to 5 at.% Sn) was found at both temperatures.

1. Introduction

The study of the magnetic behaviour of the intermetallic phases containing rare earth and magnetic transition elements such as iron or cobalt is the principal orientation in the search for the new generation of performing permanent magnets. In this context the investigation of the R–Fe–Sn ternary systems is very interesting, in particular the synthesis, composition and crystal structure peculiarity of the compounds, and phase equilibria. According to the magnetic data the $Pr_6Fe_{13}Sn$, $Nd_6Fe_{13}Sn$ and $Sm_6Fe_{13}Sn$ phases are characterized by the high temperatures of the magnetic ordering [1,2], neutron diffraction data of the RFe_6Sn_6 stannides indicate the different magnetic ordering of Fe and rare earths sublattices performed at different temperatures [3].

The isothermal sections of the phase diagrams of R–Fe–Sn ternary systems (R—rare earth element) were reported for Y, Pr, Nd, Sm, Gd and Dy [2,4–7], the preliminary investigations were carried out also for La–Fe–Sn and Lu–Fe–Sn systems [8]. Other related systems were studied only to identify isostructural series of compounds for crystallographic parameters and physical properties investigation. Two (R = La, Pr, Nd) or three (R = Sm) intermediate phases, i.e. RFe_xSn_2, $R_6Fe_{13}Sn$ and $SmFe_6Sn_6$, were observed in the systems with light rare earths, whereas for R–Fe–Sn systems, where R are heavy rare earth elements, the existence of only one ternary phase, RFe_6Sn_6, crystallising with various superstructures of the hexagonal YCo_6Ge_6-type, was found. Nevertheless, in the Lu–Fe–Sn system at higher Sn content the presence of new ternary phase $Lu_4Fe_6Sn_{19}$, identified as a cubic phase with lattice parameter $a = 1.3537$ nm, was reported in Ref. [8].

The investigation of the phase relations in the R–Fe–Sn systems is very important for understanding the influence of preparation method, heat treatment, atomic size criteria on crystal structure, number, composition and stability of formed compounds. And the next step is the sample preparation for investigation of their physical properties. In the present paper we report the isothermal sections constructed for the Er–Fe–Sn ternary system at 670 K and 770 K, the influence of heat treatment on character of the phase equilibria and for the first time, the crystal structure data for new ternary compound.

2. Experimental details

The samples were prepared by a direct arc melting of the constituent elements (erbium, purity of 99.9 wt.%; iron, purity of 99.99 wt.%; and tin, purity of 99.999 wt.%) under high purity Ti-gettered argon atmosphere on a water-cooled copper crucible. The weight losses of the initial total mass were lower than 1 wt.%. Then two pieces of the as-cast buttons were separately annealed for one month at 670 K and at 770 K in evacuated silica tubes and then water quenched.

Phase analysis was performed using X-ray powder diffraction of the synthesized samples annealed at both, 670 K and 770 K (DRON-2.0 M, Fe Kα radiation). The observed diffraction intensities were compared with reference powder patterns of binary and known ternary phases. The compositions of the obtained samples were examined by scanning electron microscopy (SEM) using REMMA-102-02 scanning microscope. Quantitative electron probe microanalysis (EPMA) of the phases was carried out by using an energy-dispersive X-ray analyser with the pure elements as standards (an acceleration voltage was 20 kV; *K*- and *L*-lines were used). The data for the crystal structure refinements were collected at room temperature using

* Corresponding author.
E-mail address: romakal@franko.lviv.ua (L. Romaka).

0925-8388/$ – see front matter © 2010 Elsevier B.V. All rights reserved.
doi:10.1016/j.jallcom.2010.07.137

Table 1
Crystallographic characteristics of the Er–Fe–Sn ternary compounds.

Compound	Structure type	Space group	Lattice parameters (nm)		
			a	*b*	*c*
$ErFe_6Sn_6$	YCo_6Ge_6	*P6/mmm*	0.53825(3)	–	0.44453(2)
*$Er_5Fe_6Sn_{18}$	$Tb_5Rh_6Sn_{18}$	*Fm-3m*	1.35676(1)	–	–

* At 670 K.

Table 2
Composition and lattice parameters of the samples of the $ErFe_xSn_2$ solid solution.

Composition	Lattice parameters (nm)			V (nm^3)
	a	*b*	*c*	
$Er_{33}Sn_{67}$	0.4365(2)	1.6132(5)	0.4285(2)	0.3017
$Er_{33}Fe_2Sn_{65}$	0.4370(1)	1.6134(2)	0.4298(1)	0.3031
$Er_{32}Fe_5Sn_{63}$ **$Er_{32.03}Fe_{5.31}Sn_{62.67}$	0.4376(1)	1.6149(2)	0.4311(1)	0.3047
*$Er_{31}Fe_7Sn_{62}$	0.4378(1)	1.6146(3)	0.4313(7)	0.3049

* Two phase sample.
** From microprobe analysis.

STOE STADI P diffractometer (graphite monochromator, Cu $K\alpha_1$ radiation). Calculations of the unit cell parameters and theoretical patterns were performed using the WinPLOTR program package [9].

3. Results and discussion

The phase equilibria in the Er–Fe–Sn phase diagram have been investigated at 670 K and at 770 K using the X-ray and metallographic analyses of 11 binary and 69 ternary alloys, annealed at both temperatures. The isothermal sections of the Er–Fe–Sn ternary system at corresponding temperatures are presented in Figs. 1 and 2, respectively. The SEM pictures and phases compositions of some alloys are shown in Fig. 3. The compositions and the crystallographic parameters of the formed compounds are listed in Table 1.

In the Fe–Sn system we confirmed the existence of the FeSn and $FeSn_2$ binaries at both 670 K and 770 K in agreement with [10,11], other two phases Fe_3Sn and Fe_3Sn_2 formed above 870 K were not observed at investigated temperatures. The Er–Sn diagram used for our investigation was taken from Ref. [10], five binary phases $ErSn_3$, $ErSn_2$, $Er_{11}Sn_{10}$, Er_5Sn_3 and Er_2Sn were observed. More recently the formation of a new phase Er_2Sn_5 prepared by induction melting was reported in Ref. [12]. During our investigation we have synthesized all the samples in the Er–Sn system with the stoichiometry corresponding to the literature data. Phase analysis of the corresponding samples confirmed a formation of $ErSn_3$, $ErSn_2$, $Er_{11}Sn_{10}$, and Er_5Sn_3 binaries under our conditions. The powder patterns of the alloys at Er_3Sn, Er_2Sn and Er_2Sn_5 stoichiometry contain two phases: $Er + Er_5Sn_3$ and $ErSn_2 + ErSn_3$, respectively.

The interstitial solid solution $ErFe_xSn_2$ (up to 5 at.% Fe) based on the $ErSn_2$ ($ZrSi_2$-type) binary compound was observed similarly

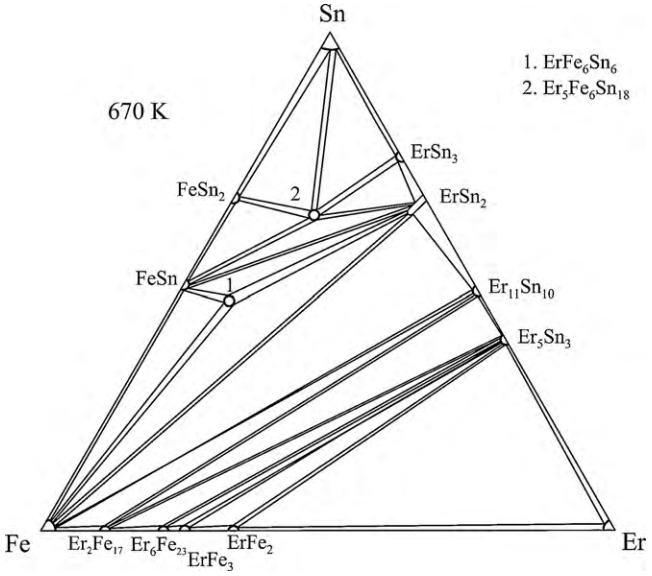

Fig. 1. Isothermal section for the Er–Fe–Sn system at 670 K.

to [13,14] (Table 2). The limit composition of this solid solution at 670 K and 770 K was estimated from the systematic analysis of the cell parameters and by the results of microprobe analysis.

According to the Refs. [10,15] the Er–Fe binary diagram was investigated above 870 K and the presence of four binary compounds Er_2Fe_{17} (Th_2Ni_{17}-type), Er_6Fe_{23} (Th_6Mn_{23}-type), $ErFe_3$ ($PuNi_3$-type) and $ErFe_2$ ($MgCu_2$-type) was found. To check the

Table 3
Crystallographic characteristics of the Er–Fe, Er–Sn and Fe–Sn binary compounds.

Compound	Structure type	Space group	Lattice parameters (nm)			Ref.
			a	*b*	*c*	
Er_2Fe_{17}	Th_2Ni_{17}	*P6$_3$/mmc*	0.8422(4)	–	0.8280(6)	This work
Er_6Fe_{23}	Th_6Mn_{23}	*Fm-3m*	1.1977(4)	–	–	This work
$ErFe_3$	$PuNi_3$	*R-3m*	0.50897(3)	–	2.4464(4)	This work
$ErFe_2$	$MgCu_2$	*Fd-3m*	0.72892(6)	–	–	This work
Er_5Sn_3	Mn_5Si_3	*P6$_3$/mcm*				[16]
$Er_{11}Sn_{10}$	$Ho_{11}Ge_{10}$	*I4/mmm*				[11]
$ErSn_2$	$ZrSi_2$	*Cmcm*	0.4365(2)	1.6132(5)	0.4285(2)	This work
$ErSn_3$	$GdSn_{2.75}$	*Amm2*	0.4336	0.4367	2.1685	[12]
FeSn	CoSn	*P6/mmm*	0.5288		0.4442	[17]
$FeSn_2$	$CuAl_2$	*I4/mcm*	0.6539		0.5325	[18]

Table 4
Atomic coordinates and isotropic displacement parameters for $ErFe_6Sn_6$ compound (space group *P*6/*mmm*, *a* = 0.53825(3), *c* = 0.44453(2) nm).

Atom	Wyckoff position	*x*/*a*	*y*/*b*	*z*/*c*	$B_{iso}\cdot10^2$ (nm^2)	Occupation
Er	1*a*	0	0	0	0.60(1)	0.449(8)
Fe	3*g*	1/2	0	1/2	0.60(1)	1
Sn1	2*c*	1/3	2/3	0	0.57(8)	1
Sn2	2*e*	0	0	0.3312(1)	0.56(1)	0.525(8)

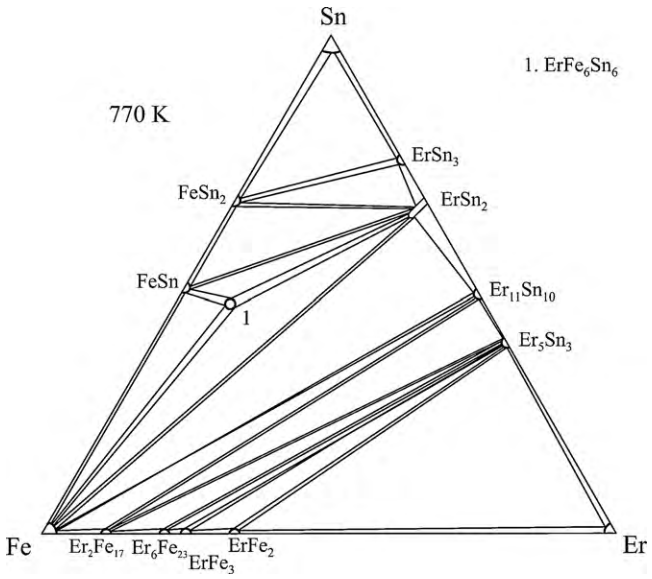

Fig. 2. Isothermal section for the Er–Fe–Sn system at 770 K.

existence of the binaries in our case, the samples of the corresponding compositions were prepared and annealed separately at 670 K and 770 K. Performed phase analysis showed the presence of the Er_2Fe_{17}, Er_6Fe_{23}, $ErFe_3$, and $ErFe_2$ phases at both investigated temperatures. The Sn solubility in the Er–Fe binary compounds was not observed. Crystallographic characteristics of the Er–Fe, Er–Sn and Fe–Sn binary compounds are presented in Table 3.

The presence of the $ErFe_6Sn_6$ stannide was confirmed at both temperatures. Taking into account the existence of two structure modifications for $ErFe_6Sn_6$ compound, reported earlier, i.e. hexagonal YCo_6Ge_6- or orthorhombic $ErFe_6Sn_6$-type [19,20], during present work, the crystal structure of this stannide was refined by X-ray powder diffraction method. Crystal structure calculations confirmed a hexagonal YCo_6Ge_6-type (space group *P*6/*mmm*, *a* = 0.53825(3), *c* = 0.44453(2) nm) for $ErFe_6Sn_6$ compound. The phase analysis of powder pattern of the corresponding ingot showed a small presence of FeSn (CoSn-type) and $ErSn_2$ ($ZrSi_2$-type) impurity phases, and they were taken into account during crystal structure calculations. The final atomic parameters, refined to $R_p = 0.028$, $R_{wp} = 0.039$, $R_{Bragg} = 0.026$, are listed in Table 4. The observed, calculated, and difference X-ray patterns for $Er_{10}Fe_{43}Sn_{47}$ sample are shown in Fig. 4 and the model of the crystal structure is presented in Fig. 5.

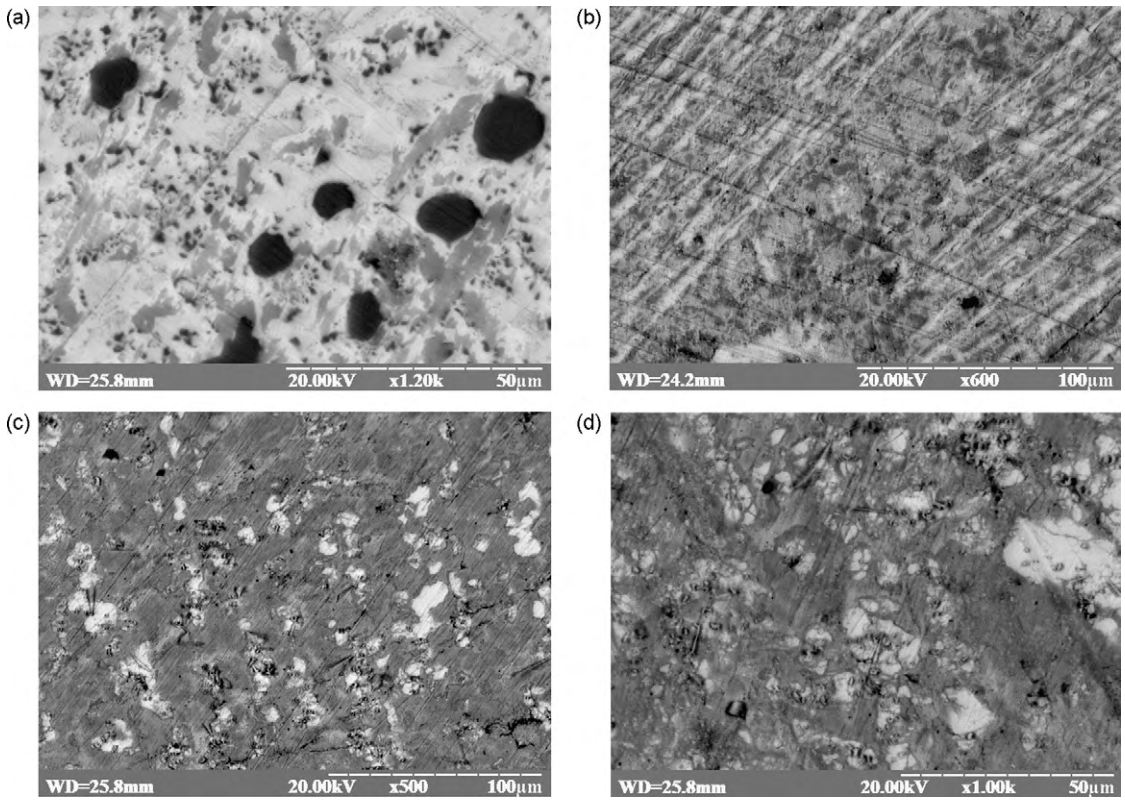

Fig. 3. Electron microphotographs of the alloys: (a) $Er_{35}Fe_{25}Sn_{40}$ (670 K)–$Er_{11}Sn_{10}$ (gray light phase); $ErSn_2$ (white phase); Fe (gray phase); (b) $Er_{20}Fe_{23}Sn_{57}$ (670 K)–$Er_5Fe_6Sn_{18}$ (gray light phase), $ErFe_xSn_2$ (white phase); FeSn (gray phase); (c) $Er_{22}Fe_{23}Sn_{55}$ (770 K)–$ErFe_6Sn_6$ (gray phase), $ErFe_xSn_2$ (white phase); (d) $Er_{25}Fe_{15}Sn_{60}$ (770 K)–FeSn (gray dark phase), $ErFe_xSn_2$ (white phase); $FeSn_2$ (gray light phase)

Table 5
Atomic coordinates and isotropic displacement parameters for $Er_5Fe_6Sn_{18}$ compound (space group *Fm*-3*m*, *a* = 1.35676(1) nm).

Atom	Wyckoff position	*x*/*a*	*y*/*b*	*z*/*c*	$B_{iso}\cdot10^2$ (nm^2)	Occupation
Er1	4*b*	0.5	0.5	0.5	1.16(7)	1
Er2	32*f*	0.1359(3)	0.1359(3)	0.1359(3)	1.44(8)	0.5
Fe	24*e*	0.2393(9)	0	0	0.74(8)	1
Sn1	32*f*	0.0951(3)	0.0951(3)	0.0951(3)	1.15(9)	0.5
Sn2	96*k*	0.1712(4)	0.1712(4)	0.5096(6)	0.52(9)	0.5
Sn3	8*c*	0.25	0.25	0.25	1.24(7)	1

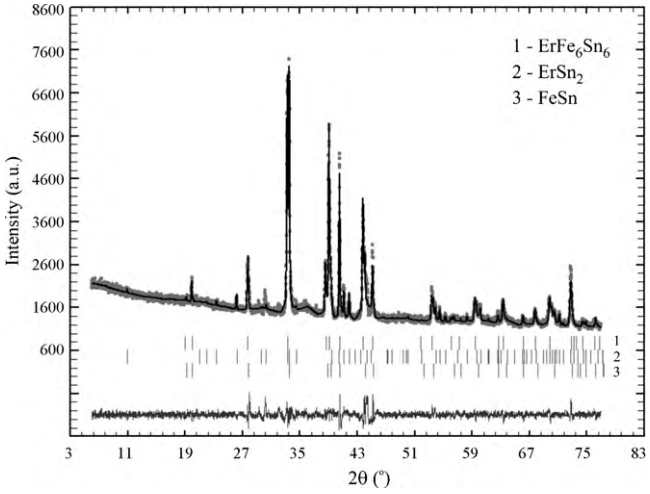

Fig. 4. The observed, calculated, and difference X-ray patterns for $Er_{10}Fe_{43}Sn_{47}$ alloy.

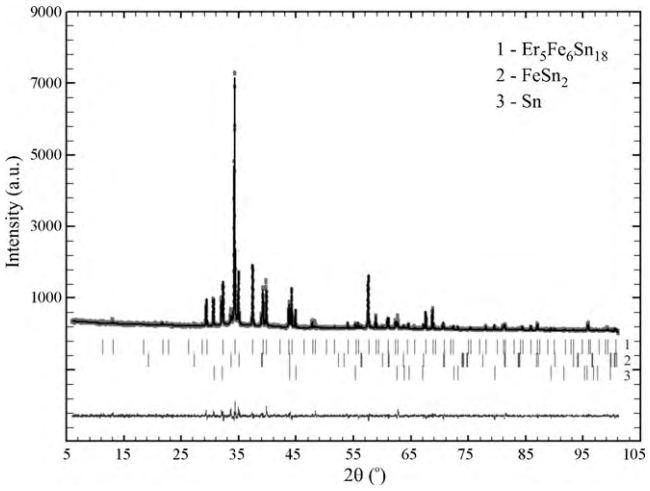

Fig. 6. The observed, calculated, and difference X-ray patterns for $Er_{15}Fe_{20}Sn_{65}$ alloy.

Structural analysis of the RFe_6Sn_6 compounds performed in Ref. [20] showed that long range ordering occurred in these phases promote a series of structures with intergrown slabs of $HfFe_6Ge_6$ and YCo_6Ge_6 or $ScFe_6Ga_6$ types. These structures are characterized by the largest orthorhombic cell related to the underlying hexagonal cell. As it was noted in Ref. [20] the orthorhombic modification of $ErFe_6Sn_6$ was established at 1123 K, while hexagonal structure with YCo_6Ge_6-type appears in $Er_{10}Fe_{43}Sn_{47}$ alloy annealed at 670 K (or 770 K), which could be explained by the existence of two modifications for $ErFe_6Sn_6$ compound. The present investigation of $ErFe_6Sn_6$ compound indicated some deviations from 1:6:6 stoichiometry, caused by deficient occupation of the Er site. Thus, we suggest that at higher temperature some structure ordering takes place in the frame of large orthorhombic cell.

The phase and metallographic analyses of the samples with Sn content more than 50 at.% result the formation of new ternary phase with approximate composition $\sim Er_{15}Fe_{20}Sn_{65}$ at 670 K, while at 770 K in the corresponding region of the Er–Fe–Sn system the phase equilibria between $FeSn_2$, FeSn and $ErSn_2$ were observed (Fig. 2).

The phase analysis performed on powder pattern of $Er_{15}Fe_{20}Sn_{65}$ sample showed that this phase appeared to be very similar to the $Er_4Rh_6Sn_{19}$-type, but structure refinements using this starting model were not satisfactory. Thus, for further crystal structure calculations the starting model of the cubic $Tb_5Rh_6Sn_{18}$ structure was chosen. The powder pattern reflections of the $Er_{15}Fe_{20}Sn_{65}$ sample were well indexed in *Fm*-3*m* space group with the cell parameter *a* = 1.35676(1) nm. The presence of weak diffraction lines belonging to $FeSn_2$ and Sn was taken into account during the crystal structure refinement of this compound. The final atomic parameters, refined to $R_p = 0.069$, $R_{wp} = 0.093$, $R_{Bragg} = 0.064$, are listed in Table 5. The observed, calculated, and difference X-ray patterns for $Er_{15}Fe_{20}Sn_{65}$ sample are shown in Fig. 6 and the model of the crystal structure is presented in Fig. 7. The obtained results are in a good agreement with the EPMA data.

The peculiarity of the crystal structure of the previous studied ternary phases RMe_xSn_y with high Sn content, where Me are Ni, Co, Ru, and Rh, is a mixture of rare earth and tin atoms in one crystallographic position. Crystal chemistry analysis of investigated $Er_5Fe_6Sn_{18}$ structure showed the full occupation of the 4*b* position

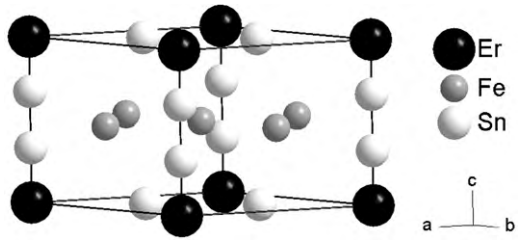

Fig. 5. The crystal structure model of the $ErFe_6Sn_6$ compound.

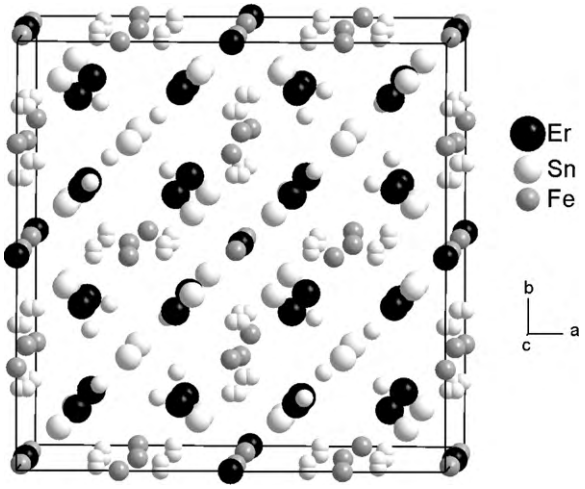

Fig. 7. The crystal structure model of the $Er_5Fe_6Sn_{18}$ compound.

exclusively by Er atoms in contrast to the $Tb_5Rh_6Sn_{18}$-type, where a statistical occupation of the 4*b* site by terbium and tin atoms was observed.

In conclusion, it should be noticed that the reduced number of the ternary phases formed in the Er–Fe–Sn system does not differ from the other R–Fe–Sn systems studied previously. On the other hand, the obtained in our work results indicated an important influence of heat treatment for ternary phases formed at high Sn content in the R–Fe–Sn systems with heavy rare earths confirmed by formation of $Er_5Fe_6Sn_{18}$ and $Lu_4Fe_6Sn_{19}$ stannides at 670 K. In this sense a close analogy in the temperature influence on character of the phase equilibria and number of formed compounds for previously investigated Gd–Cu–Sn and Dy–Cu–Sn ternary systems was observed [21,22].

References

[1] F. Weitzer, A. Leithe-Jasper, P. Rogl, K. Hiebl, H. Noel, G. Wiesinger, W. Steiner, Solid State Chem. 104 (1993) 368–376.
[2] J. Stepien-Damm, E. Galdeska, O.I. Bodak, B.D. Belan, J. Alloys Compd. 298 (2000) 26–29.
[3] J.M. Cadogan, D.H. Ryan, J. Alloys Compd. 326 (2001) 166–173.
[4] Ya. Mudryk, L. Romaka, Yu. Stadnyk, O. Bodak, D. Fruchart, J. Alloys Compd. 383 (2004) 162–165.
[5] J. Stepien-Damm, O.I. Bodak, B.D. Belan, E. Galdeska, J. Alloys Compd. 298 (2000) 169–172.
[6] P. Salamakha, P. Demchenko, O. Sologub, O. Bodak, J. Stepien-Damm, Pol. J. Chem. 71 (1997) 305–308.
[7] L.C.J. Pereira, D.P. Rojas, J.C. Waerenborgh, J. Alloys Compd. 396 (2005) 108–113.
[8] R.V. Skolozdra, in: K.A. Gschneidner Jr., L. Eyring (Eds.), Handbook on the Physics and Chemistry of Rare-Earths, vol. 24, North-Holland, Amsterdam, 1997, chapt. 164.
[9] J. Rodriguez-Carvajal, FULLPROF: A Program for Rietveld Refinement and Pattern Matching Analysis, version 3.5d; Laboratoire Léon Brillouin (CEA–CNRS), Saclay, France, 1998.
[10] T.B. Massalski, Binary Alloy Phase Diagram, ASM, Metals Park, Ohio, 1990.
[11] P. Villars, L.D. Calvert, Pearson's Handbook of Crystallographic Data for Intermetallic Phases, ASM, Metals Park, OH, 1991.
[12] A. Palenzona, P. Manfrinetti, J. Alloys Compd. 201 (1993) 43–47.
[13] G. Venturini, M. Francois, B. Malaman, B. Roques, J. Less-Common Met. 160 (1990) 215–228.
[14] M. Francois, G. Venturini, B. Malaman, B. Roques, J. less-Common Met. 160 (1990) 197–213.
[15] A. Maeyer, A.G. Siemens, J. Less-Common Met. 18 (1969) 41–48.
[16] W. Jeitschko, E. Parthe, Acta Crystallogr. 22 (1967) 551–555.
[17] K. Yamaguchi, H. Watanabe, J. Phys. Soc. Japan 22 (1967) 1210–1213.
[18] E.E. Navinga, H. Damsma, P. Hokkeling, J. Less-Common Met. 27 (1972) 169–186.
[19] O.E. Koretskaya, R.V. Skolozdra, Inorg. Mater. 22 (1986) 606–607.
[20] B.C. Idrissi, G. Venturini, B. Malaman, Mater. Res. Bull. 26 (1991) 1331–1338.
[21] L. Romaka, V.V. Romaka, E.K. Hlil, D. Fruchart, Chem. Met. Alloys 2 (1,2) (2009) 68–74.
[22] V. Romaka, Yu. Gorelenko, L. Romaka, Visnyk Lviv Univ. 49 (2008) 3–9.